JOURNAL OF AIRCRAFT
Vol. 37, No. 4, July–August 2000

Unsteady Aerodynamics of a Wing-in-Ground-Effect Airfoil Flying over a Wavy Wall

Ye-Hoon Im* and Keun-Shik Chang†
Korea Advanced Institute of Science and Technology, Taejon 305-701, Republic of Korea

Aerodynamic characteristics of an airfoil, the NACA 6409, flying over a wavy wall is investigated numerically. An Euler code based on the *LU*-factored algorithm and higher-order upwind scheme is constructed and its accuracy is tested with three benchmark problems: a NACA 4412 airfoil moving over a level ground, a NACA 0012 airfoil in free-flight pitching oscillation, and a NACA 0012 airfoil flying over a wavy wall. The calculated flow about NACA 6409 airfoil over the wavy ground represented by a moving sine function indicates that the aerodynamic property of the airfoil becomes sensitive if the wave number or amplitude of the wavy ground is increased and/or if the proximity of the airfoil to the ground is lowered.

Nomenclature

A, B = Jacobians of flux vector E and F: $A = \partial \bar{E}/\partial \bar{Q}$, $B = \partial \bar{F}/\partial \bar{Q}$
a = nondimensional wave amplitude
C_l = lift coefficient
C_{lo} = lift coefficient of incompressible flow
$C_{m1/4}$ = pitching moment coefficient about the quarter-chord point: positive for pitch-up moment
C_n = normal force coefficient
C_p = pressure coefficient
D_ξ, D_η = differential operator in ξ and η directions
$\bar{E}$, $\bar{F}$ = flux vectors E and F expressed in the body-fitted coordinate system
e = elevation of free surface (EFS) at the airfoil leading edge
e_t = total energy
g = gravitational acceleration
H = depth of water
h = elevation of airfoil
J = transformation Jacobian
k = wave number
M_∞ = flight Mach number
n = unit normal vector
p = pressure
$\bar{Q}$ = conservation vector Q expressed in the body-fitted coordinate system
S_a, S_b = eigenvectors of matrix A and B, respectively
T = period
t = time
U_g = grid velocity
U_∞ = speed of the airfoil
u, v = velocity component in the (x, y) coordinates
X_{cp} = the coordinate for center of pressure
x_t, y_t = velocity of a grid point in x and y directions
α = angle of attack
Λ_a, Λ_b = eigenvalue matrix for the matrix A and B, respectively
λ = wavelength
λ_a, λ_b = eigenvalue of matrix A and B, respectively
ξ, η = body-fitted coordinate system
ρ = density

Received 26 August 1999; revision received 12 January 2000; accepted for publication 14 January 2000.

*Graduate Student, Department of Aerospace Engineering.
†Professor, Department of Aerospace Engineering, 373-1 Kusong-Dong, Yusong-ku. Member AIAA.

Introduction

WHEN an aircraft flies near the ground, the aerodynamic properties of the wing are naturally altered from that of the free flight. In particular, a wing in proximity to the ground manifests reduced upwash, downwash, and tip vortices, which cause enhancement of lift and pitching moment and reduction of induced drag. These effects are called the ground effect, whereas the wing taking advantage of these effects is called a wing in ground effect (WIG). There has been recently considerable interest in development of WIG crafts in such countries as Russia,[1,2] Japan,[3,4] Germany,[5,6] and China[7] because of its energy-saving feature as a means of passenger and cargo transportation. Preliminary design of a WIG airplane is under progress in South Korea,[8] and the present research is motivated by this particular program.

The gain in the lift-to-drag ratio might be achieved by a WIG craft at the cost of stability because of the increased pitching moment. The flight properties of a WIG hence need to be thoroughly investigated in the development process. Recently, a few reports have appeared on the performance of WIG wings and airfoils[4–7,9] flying over a level ground. NACA four-digit airfoils are, in general, known to have positive ground effect. However, a symmetric airfoil with large thickness, the NACA 0012 for example, can exhibit negative ground effect at a small angle of attack.[4,7] The WIG craft operated over the sea is expected to encounter rough wavy surfaces from time to time. This rather periodic terrain will cause ground effect different from that of the level ground.

In the literature the unsteady flow past a two-dimensional airfoil moving over a wavy ground has been investigated with the lifting surface theory by Ando et al.[10] and with the unsteady panel method by Morishita and Ashihara.[11] Mizutani and Suzuki[12] used Rankine source and boundary element methods to compute the wing aerodynamics over the free surface. Their results offer useful data for fundamental study of the lifting airfoils. However, the solutions of Euler and Navier–Stokes equations are still wanted to investigate the compressibility and viscosity effect on the WIG craft.

In this paper the Euler equations with the *LU*-factored algorithm[13] and high-resolution upwind scheme have been numerically solved for the unsteady WIG airfoil moving over a wavy wall. Mizutani and Suzuki[12] have found that deformation of the free surface caused by the proximate flight of a WIG craft is only negligible. The accuracy of the present computer code has been verified by reproducing the earlier WIG result of Hayashi and Endo.[14] Particularly, to check the time accuracy of the code the NACA 0012 airfoil in pitching oscillation[15] is solved. Parameteric effect of NACA 6409 airfoil flying over a wavy wall at a subsonic flight Mach number $M_\infty = 0.3$ is elaborated in this paper.

Governing Equations

The unsteady two-dimensional Euler equations in the computational domain (t, ξ, η) are considered.

$$\frac{\partial \bar{Q}}{\partial t} + \frac{\partial \bar{E}}{\partial \xi} + \frac{\partial \bar{F}}{\partial \eta} = 0 \tag{1}$$

with the flux vectors

$$\bar{E} = (1/J)(\xi_t Q + \xi_x E + \xi_y F), \qquad \bar{F} = (1/J)(\eta_t Q + \eta_x E + \eta_y F)$$

where

$$J = 1/(x_\xi y_\eta - x_\eta y_\xi), \qquad Q = [\rho, \rho u, \rho v, \rho e_t] = J\bar{Q}$$

$$E = [\rho u, \rho u(u - x_t) + p, \rho(u - x_t)v, \rho e_t(u - x_t) + pu]$$

$$F = [\rho v, \rho u(v - y_t), \rho v(v - y_t) + p, \rho e_t(v - y_t) + pv]$$

To obtain second-order accuracy in time, Eq. (1) is discretized as

$$\frac{\bar{Q}^{n-1} - 4\bar{Q}^n + 3\bar{Q}^{n+1}}{2\Delta t} + D_\xi \bar{E}^{n+1} + D_\eta \bar{F}^{n+1} = 0 \tag{2}$$

The nonlinear flux vectors in Eq. (2) are locally linearized using the Jacobian matrices. The result is

$$\frac{3\delta\bar{Q}^n - \delta\bar{Q}^{n-1}}{2\Delta t} + (D_\xi A + D_\eta B)\delta\bar{Q}^n + D_\xi \bar{E}^n + D_\eta \bar{F}^n = 0 \tag{3}$$

where

$$\delta\bar{Q}^n = \bar{Q}^{n+1} - \bar{Q}^n, \qquad \delta\bar{Q}^{n-1} = \bar{Q}^n - \bar{Q}^{n-1}$$

The Jacobian matrices A and B are respectively split into A^+ and A^- and B^+ and B^-. One-side difference in the upwind direction for the spatial derivatives is then applied. The result is

$$\left[3I + 2\Delta t\left(A_i^+ - A_i^- + B_j^+ - B_j^-\right)\right]\delta\bar{Q}^n - 2\Delta t\left(A_{i-1}^+ + B_{j-1}^+\right)\delta\bar{Q}^n + 2\Delta t\left(A_{i+1}^- + B_{j+1}^-\right)\delta\bar{Q}^n = \delta\bar{Q}^{n-1} - 2\Delta t\left(D_\xi \bar{E}^n + D_\eta \bar{F}^n\right) \equiv R \tag{4}$$

where

$$A^\pm = S_a^+ \Lambda_a^\pm S_a^-, \qquad \Lambda_a^\pm = \mathrm{diag}[(\lambda_a \pm |\lambda_a|)/2]$$

$$B^\pm = S_b^+ \Lambda_b^\pm S_b^-, \qquad \Lambda_b^\pm = \mathrm{diag}[(\lambda_b \pm |\lambda_b|)/2]$$

In Eq. (4) the diagonal, lower triangular, and upper triangular operator groups are identified and they are denoted by D, L, and U, respectively. Equation (4) then simply becomes

$$(D + L + U)\delta\bar{Q}^n = -R \tag{5}$$

where

$$D = \left[3I + 2\Delta t\left(A_i^+ - A_i^- + B_j^+ - B_j^-\right)\right]$$

$$L = -2\Delta t\left(A_{i-1}^+ - B_{j-1}^+\right), \qquad U = 2\Delta t\left(A_{i+1}^- + B_{j+1}^-\right)$$

Equation (5) is solved by the two LU solution steps:

$$(D + L)\delta\bar{Q}^* = -R, \qquad (D + U)\delta\bar{Q} = D\delta\bar{Q}^* \tag{6}$$

where

$$\bar{Q}^{n+1} = \bar{Q}^n + \delta\bar{Q}$$

Wall Boundary Conditions and Grid

The density and pressure on the wavy wall are extrapolated in the normal direction from the field solution of the earlier time step. The slip velocity satisfies the flow-tangency condition

$$(\boldsymbol{U} - \boldsymbol{U}_g) \cdot \boldsymbol{n} = 0$$

The wavy wall is modeled by a traveling sine function. Using the coordinate transformation $X = x - U_\infty t$, the vertical distance traveled by a point at x on the moving wave, during a small time step $\mathrm{d}t$, is

$$\mathrm{d}y = a \cdot \{\sin[(2\pi/\lambda)(X - U_\infty\, \mathrm{d}t)] - \sin[(2\pi/\lambda)X]\}$$

Then the location of the inner grid points in the computational domain can be readjusted at each time step by the spring analogy.[16]

Computational Results

Code Validation

The existing result of a NACA 4412 airfoil moving over a level ground is reproduced first. Total 77×2 grid points are distributed on the airfoil, and a two-block H-grid system is used with 141×32 and 141×45 grid points, respectively. The flow velocity in the wind-tunnel experiment by Hayashi and Endo[14] was 20 m/s. The Mach number was $M_\infty = 0.059$, and Reynolds number was $Re = 3.2 \times 10^5$ based on the airfoil chord length. Nondimensional elevation of the airfoil at the midchord, above the flat surface, was $h = 0.4$. The present computation was made with Mach number $M_\infty = 0.2$. The similarity rule $C_l = C_{l_0}/\sqrt{(1 - M_\infty^2)}$ can be opted for data shift between different Mach numbers. The angle of attack was increased by one degree up to $\alpha = 8.0$ deg for computation. Figure 1 verifies that the present lift coefficient is in good agreement with the experimental data[14] at $\alpha = 0.0$ and 4.0 deg, but shows a little deviation at the highest angle of attack $\alpha = 8.0$ deg because of the increased boundary-layer effect. Figure 2 shows the pressure contours at the angle of attack $\alpha = 4$ deg, suggesting a rather uniform flow beneath the flat lower surface and high acceleration above the curved upper surface.

To check the time accuracy, freestream Mach number 0.8 is considered for the NACA 0012 airfoil in pitching oscillation about 25% chord length, which follows as

$$\alpha = \alpha_0 + \alpha_1 \sin(\omega t)$$

where $\alpha_0 = 0$ deg, $\alpha_1 = 5$ deg, and $\omega = 1.90$. A two-block H-type grid system with 129×33 grid points are used. Figure 3a shows cyclic change of the normal force coefficient calculated with 96

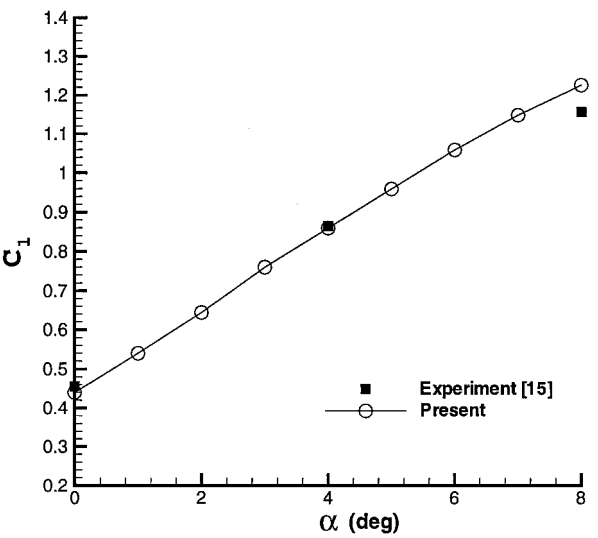

Fig. 1 Lift coefficient of the NACA 4412 airfoil over a level ground: $h = 0.4$ and $M_\infty = 0.2$.

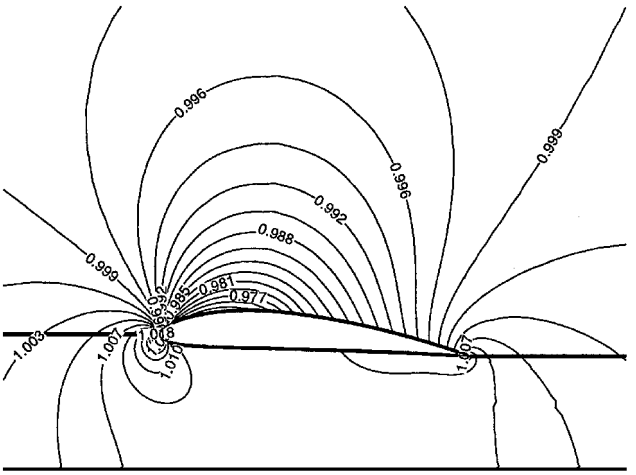

Fig. 2 Pressure contours around the NACA 4412 airfoil: M_∞ = 0.2 and α = 4.0 deg.

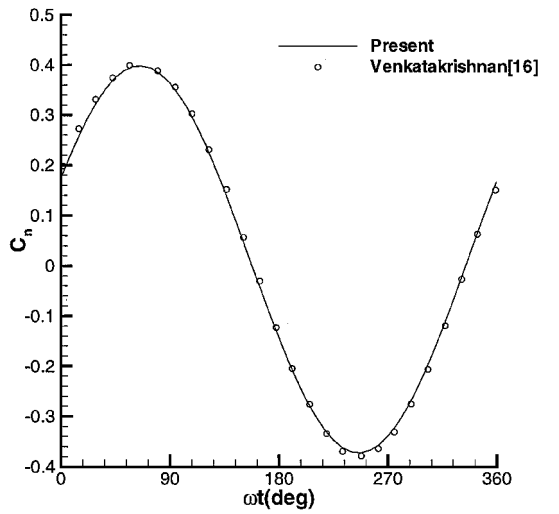

a) Cyclic normal force coefficient

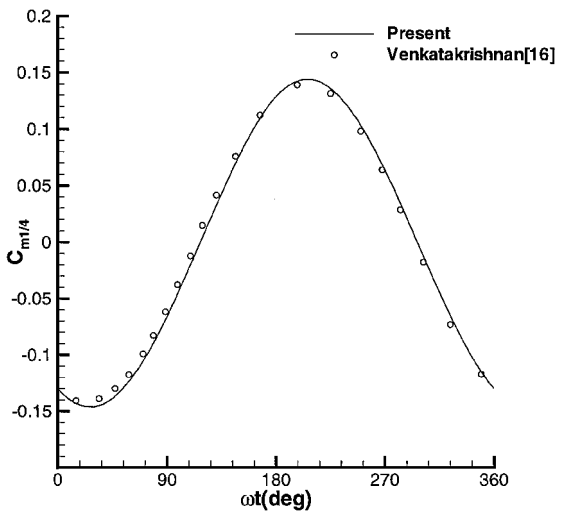

b) Pitching moment coefficient

Fig. 3 M_∞ = 0.8 with α = 5.0 deg $\times$ sin(1.9t).

time steps per cycle, which gives good comparison with the existing result.[15] At the phase angle 67.5 deg the normal force coefficient hits the maximum value 0.3972 at $\alpha = 4.62$ deg; at the phase angle 247.5 deg, the minimum value -0.3734 is reached with $\alpha = -4.62$ deg. Figure 3b shows the pitching moment coefficient about the quarter chord length. Its minimum occurs at $\alpha = 2.5$ deg with phase angle 30 deg, and its maximum at $\alpha = -2.5$ deg with phase angle 210 deg.

A NACA 0012 airfoil flying over a wavy wall at $\alpha = 0.0$ deg with Mach number $M_\infty = 0.2$ was calculated to compare with Morishita and Ashihara's result.[11] Airfoil elevation is 0.5, and wave amplitude is 0.2, while the wavelength is varied from 1.5 to 4.0. Figure 4 shows the average lift coefficient variation with respect to the wavelength. The panel method shows good agreement up to the wavelength $\lambda = 3.0$, but shows deviation afterward.

WIG Airfoil over the Wavy Wall

According to the observation data collected by the Korea Oceanographic Data Center, the most common waves in Korean coastal waters have a range of amplitude 0.2 ~ 5 m and period 4 ~ 8 s. The dispersion relation[17] can be used to relate the period T, wavelength λ, and wave number k by

$$T = 2\pi / gk \tanh(kH)$$

where $k = 2\pi/\lambda$. The range of wavelength is then between 25 and 100 m. Using the variables scaled by the airfoil chord length, the following parameter range received our attention: airfoil elevation $h = 0.1 \sim 0.3$, wave amplitude $a = 0.025 \sim 0.1$, and wavelength $\lambda = 1.5 \sim 5.0$. In 5–15 periods with 4500 ~ 9000 time steps per one period depending on the parameters, the numerical solution converged. Figure 5 depicts the geometric parameters used in the present problem.

Case 1: Wavy Wall with h = 0.1 and a = 0.025

The NACA 6409 airfoil with three different wavelengths is considered: $\lambda = 1.5$, 3.0, and 5.0. We used a two-block H-grid system: 241 $\times$ 25 grid points below the airfoil and 241 $\times$ 45 above the airfoil and 144 grid points on the airfoil itself. Figure 6 shows the cyclic variation of C_n, as a function of e, the elevation of free surface (EFS) at the leading edge of the airfoil. When the EFS is increasing from negative to positive or the airfoil is moving toward the crest (see curve a of Fig. 7) pressure builds up on the lower surface of the

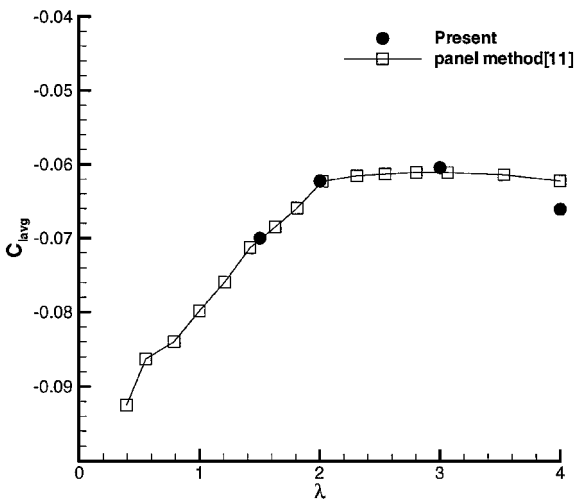

Fig. 4 NACA 0012 airfoil over a wavy wall: average lift coefficient vs wavelength.

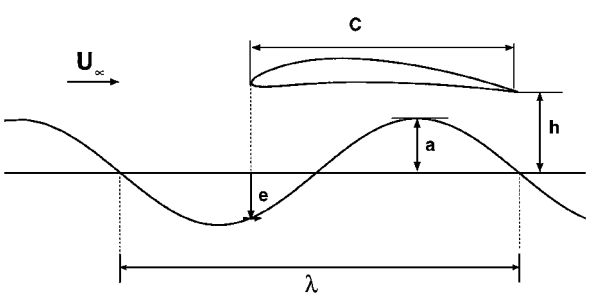

Fig. 5 WIG geometry.

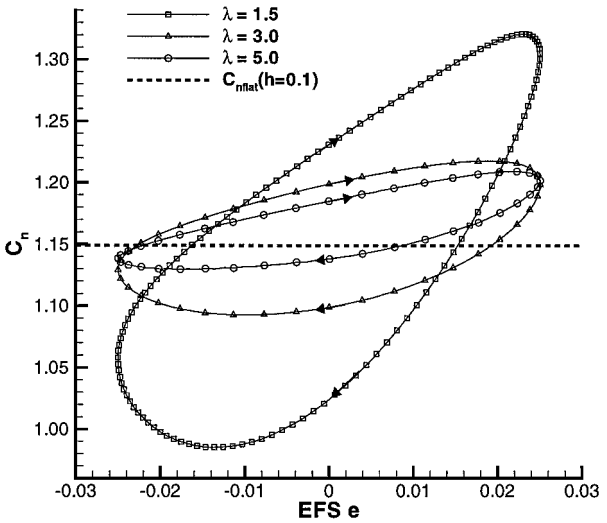

Fig. 6 Phase curve for C_n: case 1.

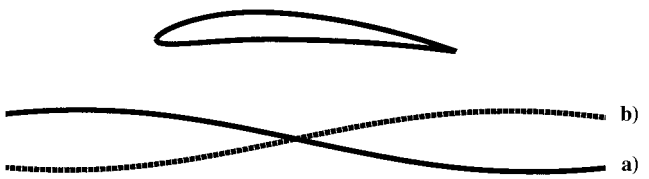

Fig. 7 Airfoil flying over a wavy wall: a) EFS increasing and b) EFS decreasing.

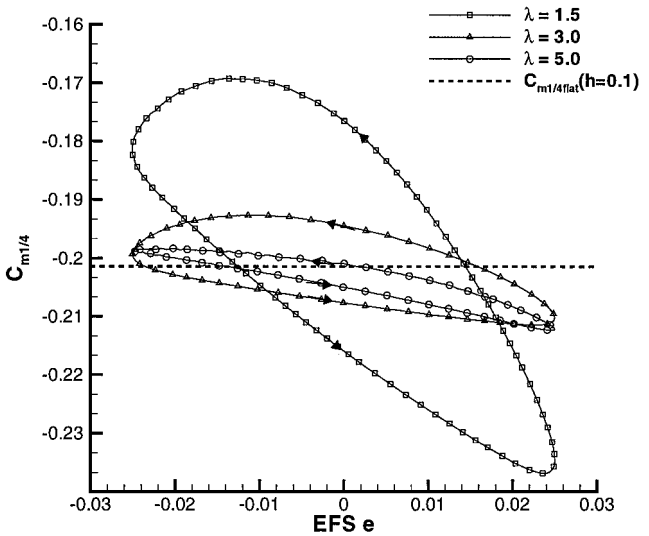

Fig. 8 Phase curve for $C_{m1/4}$: case 1.

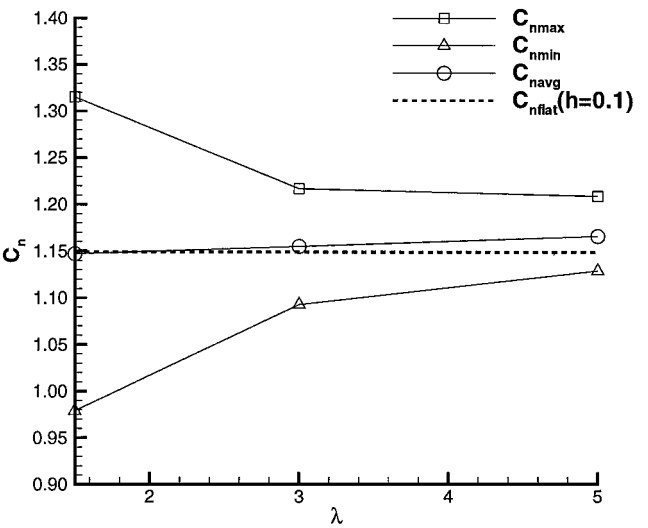

Fig. 9 C_n vs wavelength: case 1.

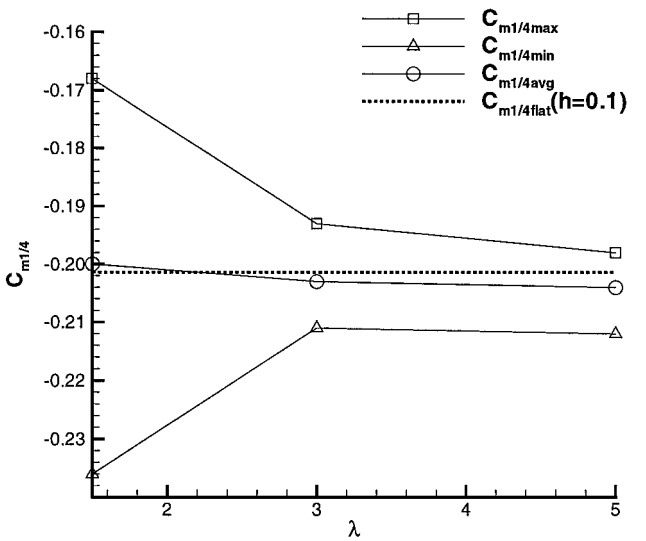

Fig. 10 $C_{m1/4}$ vs wavelength: case 1.

airfoil, escalating the normal force coefficients. When the EFS is decreasing or the airfoil is moving away from the crest (see curve b of Fig. 7) the situation is reversed. This effect is seen from the positive slope of the phase curves in Fig. 6. The all-negative pitching moment $C_{m1/4}$ in Fig. 8 shows an opposite property. Because the phase curves have negative slopes, $C_{m1/4}$ decreases when the airfoil moves toward the crest and increases when it moves away from the crest. Both Figs. 6 and 8 indicate that the phase curves are very sensitive for the short wavelength waves. Figures 9 and 10 give maximum, minimum, and average values of the aerodynamic coefficients. The normal force coefficient C_n undergoes 29.3% fluctuation from its average value with the shortest wavelength $\lambda = 1.5$; a lower 10.7% fluctuation with the medium wavelength $\lambda = 3.0$; and a meager 6.9% fluctuation with the longest wavelength $\lambda = 5.0$. Similarly, the pitching moment coefficient $C_{m1/4}$ undergoes corresponding 34.0, 8.7, and 6.9% fluctuations, respectively. Figure 11 shows distribution of the surface pressure coefficient at different times plotted for the wavelength $\lambda = 1.5$. It indicates that pressure variation is slight on the upper surface of the airfoil, whereas it is significant on the lower surface. Figure 12 shows geometric fluctuation of the center of pressure. For the shortest wavelength $\lambda = 1.5$ the slope of the curve is steep, and two crossover points are observed. The cyclic fluctuation of both C_n and $C_{m1/4}$ is as much as 30%, but X_{cp} is changed by meager 1% because the phase curves of C_n and $C_{m1/4}$ have opposite slopes.

Case 2: Wavy Wall with $h = 0.3$ and $a = 0.025$

The consequence of higher airfoil elevation is now examined with $\lambda = 1.5$, 3.0, and 5.0. Two grid systems, 241 × 33 and 241 × 42, are used. Figure 13 shows the phase curve of C_n, which is also plotted in Fig. 14. For the wavelength $\lambda = 1.5$, C_n varies from 0.996 to 1.051 or shows 5.4% fluctuation. For the wavelength $\lambda = 3.0$, C_n is in the range 0.997 ~ 1.034, showing 3.7% fluctuation. For $\lambda = 5.0$, C_n is between 1.002 ~ 1.024 with 2.2% fluctuation. C_n is not much changed from that of the level ground. Figures 15 and 16 indicate that $|C_{m1/4}|$ is in the range 0.169 ~ 0.180 for $\lambda = 1.5$, in 0.171 ~ 0.175 for $\lambda = 3.0$, and in 0.172 ~ 0.174 for $\lambda = 5.0$. Corresponding fluctuation of amplitude is 6.3, 2.3, and 1.1%, respectively. Figure 17 shows that the center of pressure is moved between 0.4193 ~ 0.4223. These curves appear rugged because their scale is significantly magnified. For $\lambda = 1.5$, as the airfoil approaches the

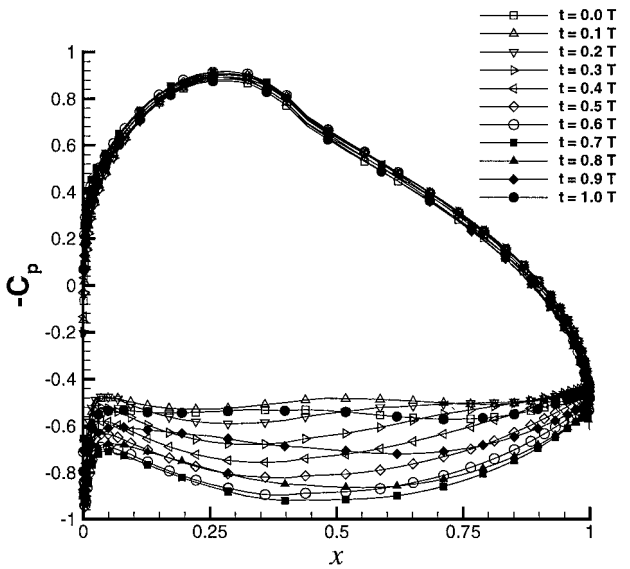

Fig. 11 Pressure coefficient distribution: $\lambda = 1.5$ (case 1).

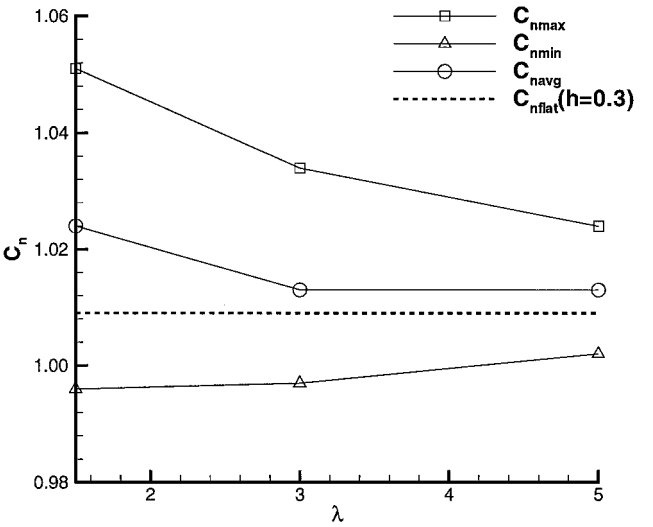

Fig. 14 C_n vs wavelength: case 2.

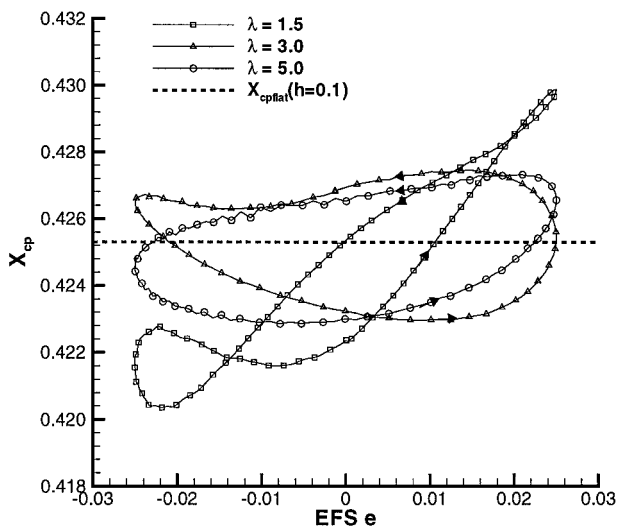

Fig. 12 Phase curve for the center of pressure: case 1.

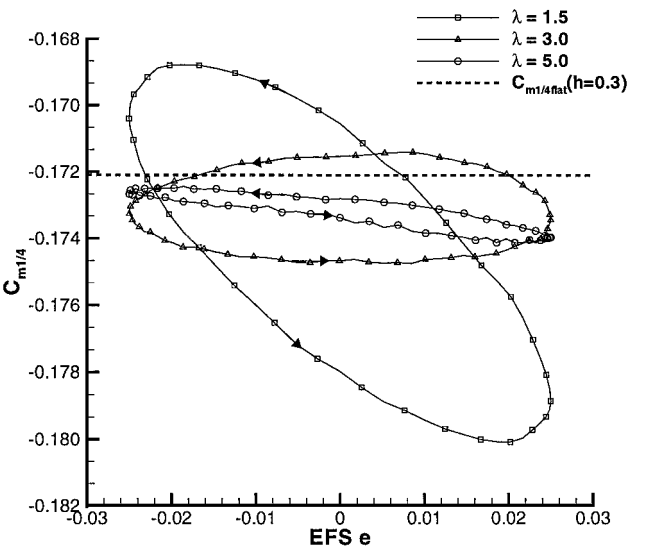

Fig. 15 Phase curve for $C_{m1/4}$: case 2.

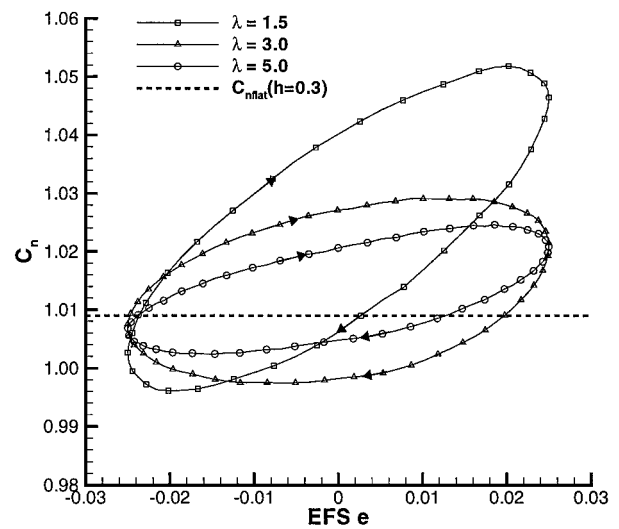

Fig. 13 Phase curve for C_n: case 2.

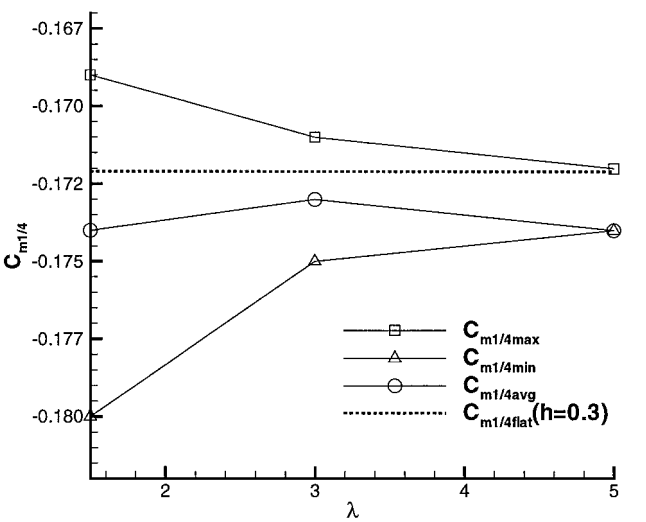

Fig. 16 $C_{m1/4}$ vs wavelength: case 2.

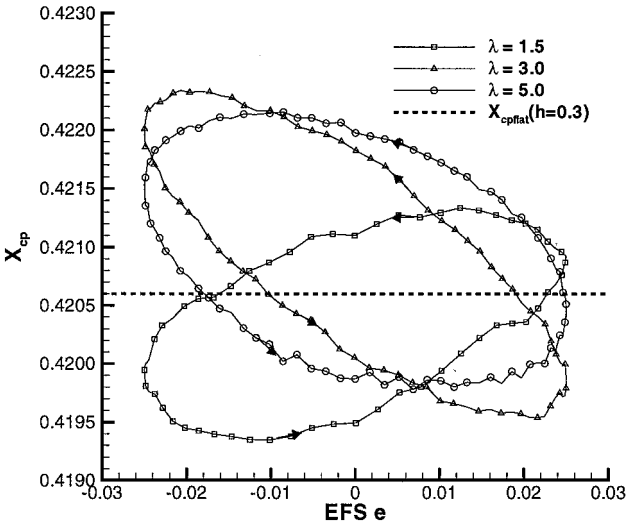

Fig. 17 Phase curve for the center of pressure: case 2.

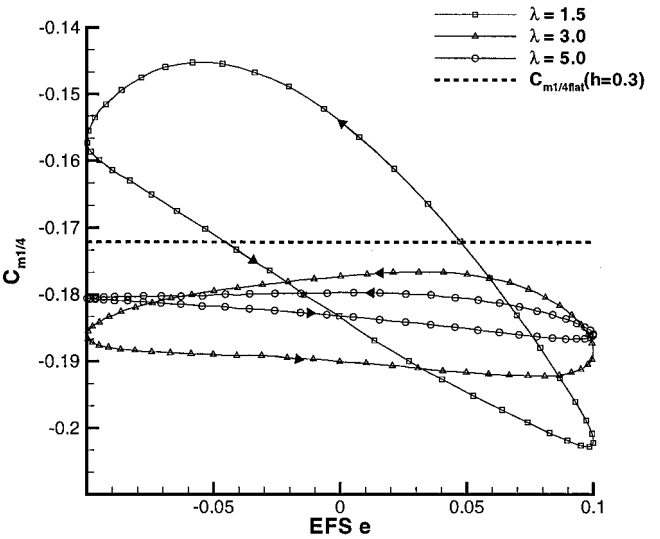

Fig. 20 Phase curve for $C_{m1/4}$: case 3.

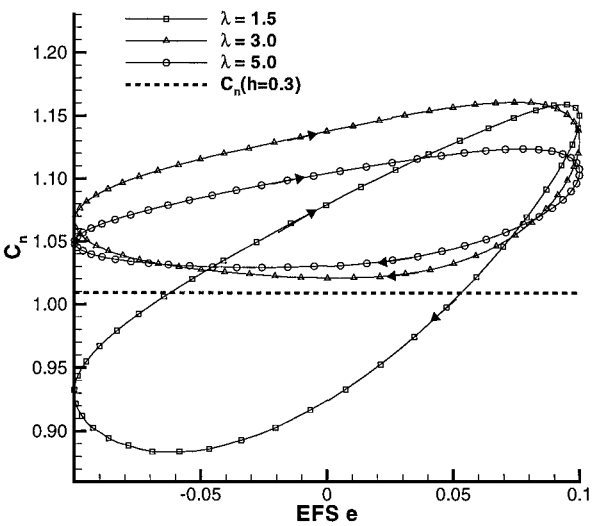

Fig. 18 Phase curve for C_n: case 3.

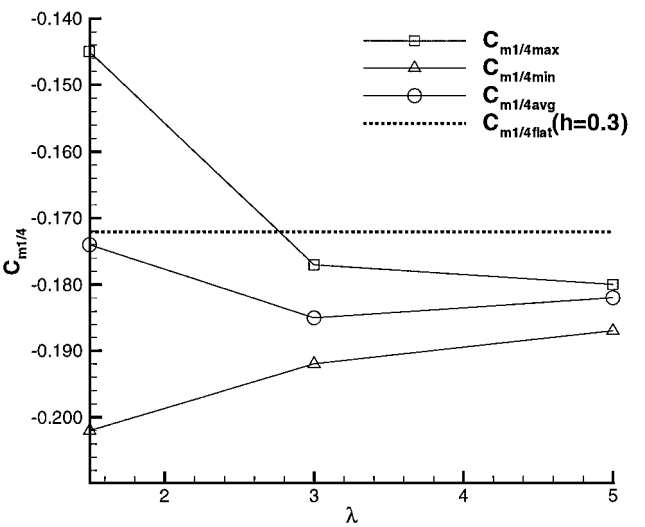

Fig. 21 $C_{m1/4}$ vs wavelength: case 3.

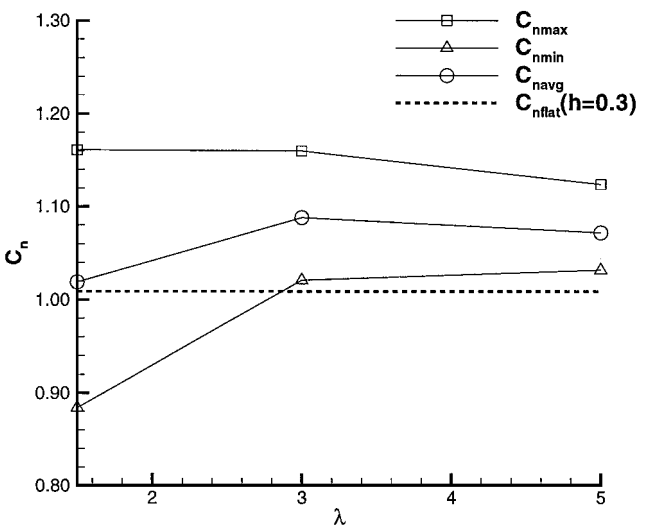

Fig. 19 C_n vs wavelength: case 3.

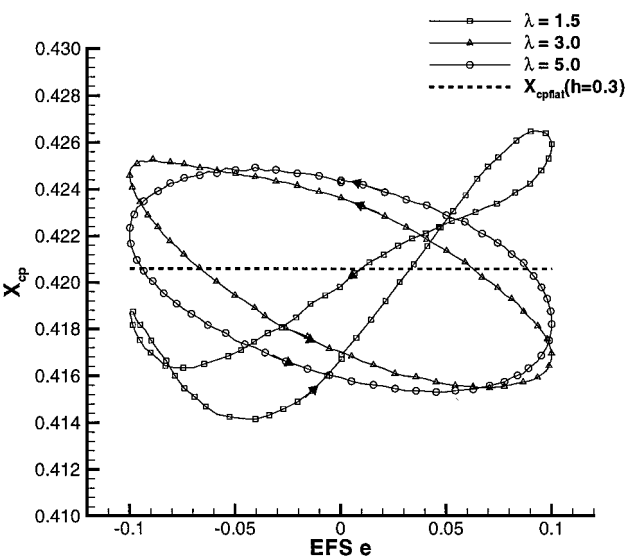

Fig. 22 Phase curve for the center of pressure: case 3.

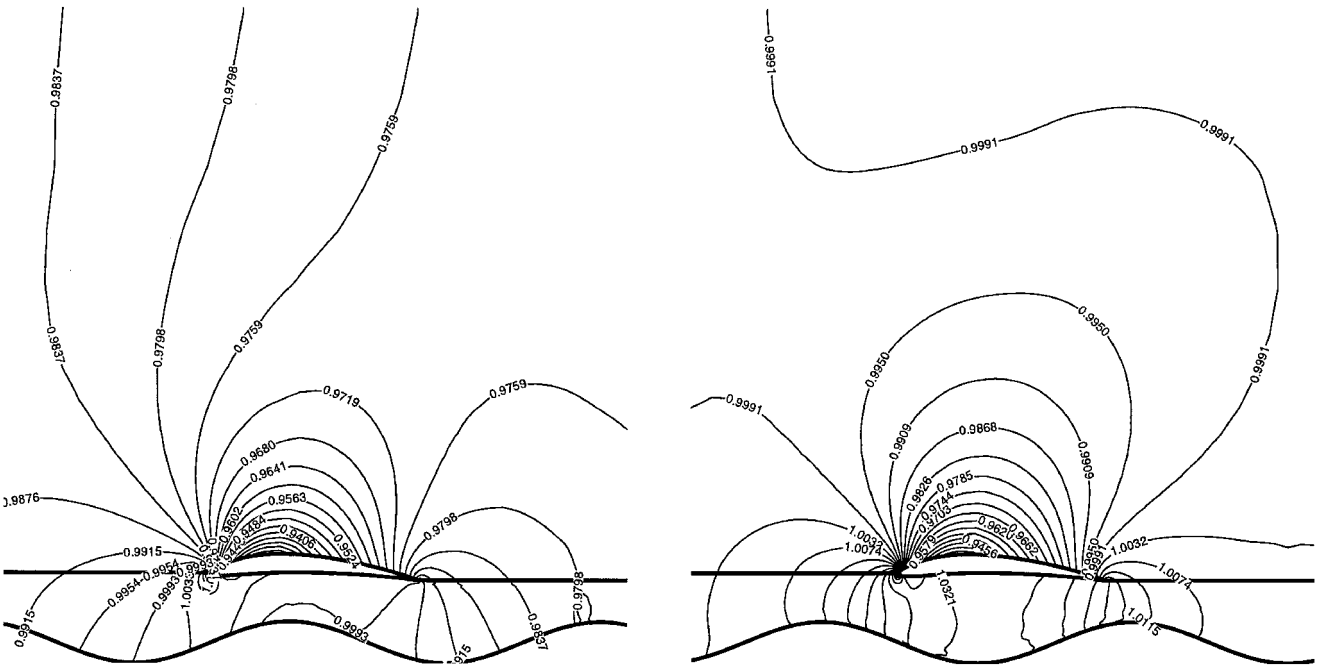

Fig. 23 Pressure contours.

crest, X_{cp} is moved a little toward the trailing edge of the airfoil and vice versa. However for $\lambda = 3.0$ and 5.0 the motion of X_{cp} is reversed. For convergence of the solution or for closure of the phase curves, an increased number of iteration was necessary in case 2 rather than in case 1.

Case 3: Wavy Wall with $h = 0.3$ and $a = 0.1$

Significant fluctuation of the aerodynamic coefficients are observed with this large wave amplitude and short wavelengths. Figures 18 and 19 show that C_n undergoes 27.2, 12.8, and 8.6% fluctuation for $\lambda = 1.5$, 3.0, and 5.0, respectively. The pitching moment coefficient $C_{m1/4}$ in Figs. 20 and 21 shows fluctuation as high as 32.8, 8.1, and 3.8%, respectively. Figure 22 depicts that the geometric excursion of the center of pressure is made in the range $0.4124 \sim 0.4253$. Figure 23 represents the instantaneous pressure contours at two different instants of a period. For the flight Mach number $M_\infty = 0.3$ and wavelength $\lambda = 1.5$, the cyclic load has an equivalent frequency $f = 11.36$ Hz in the physical space. This would result in severe structural fatigue problem and discomfort of passengers unless the WIG craft is properly controlled.

Conclusions

The numerical solution of the Euler equations by the *LU*-factored scheme has availed the aerodynamic data for the WIG airfoil moving over a wavy wall. The numerical results showed good agreement with the existing reports on the three benchmark problems: a NACA 4412 airfoil over a level ground, a NACA 0012 airfoil in free-flight pitching oscillation, and a NACA 0012 airfoil over a wavy wall. For the analysis of the parametric effect of the wavy wall on the flight of NACA 6409 airfoil, two airfoil elevations $h = 0.1$ and 0.3, two wave amplitudes $a = 0.025$ and 0.01, and three wave lengths $\lambda = 1.5$, 3.0, and 5.0 were investigated. For the shortest wavelength $\lambda = 1.5$, the phase curves of aerodynamic coefficients showed steepest slope for all of the airfoil elevations and wave amplitudes. However, rather flat phase curves have been obtained for the larger wavelengths $\lambda = 3.0$ and 5.0.

References

[1]Alexeyev, S. S., "Creation of High-Speed Amphibious Boats Using Ground Proximity Effect of the Example of Sever Boats," *Workshop Proceedings of Ekranoplans and Very Fast Craft*, Australian Maritime Eng. CRC Ltd., Univ. of New South Wales, Sydney, Australia, 1996, pp. 134–145.

[2]Kirillovihk, V. N., and Privalov, E. I., "Transport Amphibious Platforms: A New Type of High-Speed Craft," *Workshop Proceedings of Ekranoplans and Very Fast Craft*, Australian Maritime Eng. CRC Ltd., Univ. of New South Wales, Sydney, Australia, 1996, pp. 121–133.

[3]Ando, S., "Critical Review of Design Philosophies for Recent Transport WIG Effect Vehicles," *Japan Society for Aeronautical and Space Science Transactions*, Vol. 33, No. 99, 1990, pp. 28–40.

[4]Morishita, E., and Tezuka, K., "Ground Effect Calculation of Two-Dimensional Airfoil," *Japan Society for Aeronautical and Space Science Transactions*, Vol. 36, No. 114, 1994, pp. 270–280.

[5]Steinbach, D., and Jacob, K., "Some Aerodynamic Aspects of Wings Near Ground," *Japan Society for Aeronautical and Space Science Transactions*, Vol. 34, No. 104, 1991, pp. 56–70.

[6]Jacob, K., "Advanced Method for Computing Flow Around Wings with Rear Separation and Ground Effect," *Journal of Aircraft*, Vol. 24, No. 2, 1987, pp. 126–128.

[7]Hsiun, C. M., and Chen, C. K., "Aerodynamic Characteristcs of a Two Dimensional Airfoil with Ground Effect," *Journal of Aircraft*, Vol. 33, No. 2, 1996, pp. 386–392.

[8]Shin, M. S., and Yang, S. I., "Performance Prediction of the Eight-Passenger Class Wing-In-Ground Effect Ship," *Workshop Proceedings of Ekranoplans and Very Fast Craft*, Australian Maritime Eng. CRC Ltd., Univ. of New South Wales, Sydney, Australia, 1996, pp. 108–120.

[9]Plotkin, A., and Dodbele, S. S., "Slender Wing in Ground Effect," *AIAA Journal*, Vol. 26, No. 4, 1988, pp. 493, 494.

[10]Ando, S., Sakai, T., and Nitta, K., "Analysis of Motion of Airfoil Flying over Wavy-Wall Surface," *Japan Society for Aeronautical and Space Science Transactions*, Vol. 35, No. 107, 1992, pp. 27–38.

[11]Morishita, E., and Ashihara, K., "Ground Effect Calculation of a Two-Dimensional Airfoil over a Wavy Surface," *Japan Society for Aeronautical and Space Science Transactions*, Vol. 38, No. 119, 1995, pp. 77–90.

[12]Mizutani, N., and Suzuki, K., "Numerical Analysis of 3-D WIG Advancing over the Still Water Surface," *Journal of Society of Naval Architects of Japan*, Vol. 174, No. 1, 1993, pp. 35–45.

[13]Shuen, J. S., "Upwind Differencing and LU Factorization for Chemical Non-Equilibrium Navier–Stokes Equations," *Journal of Computational Physics*, Vol. 99, No. 2, 1992, pp. 233–250.

[14]Hayashi, M., and Endo, E., "Measurement of Flow Fields Around an Airfoil Section with Separation," *Japan Society for Aeronautical and Space Science Transactions*, Vol. 21, No. 52, 1978, pp. 69–75.

[15]Venkatakrishnan, V., and Jameson, A., "Computation of Unsteady Transonic Flows by the Solution of Euler Equations," *AIAA Journal*, Vol. 26, No. 8, 1988, pp. 974–981.

[16]Robinson, B. A., Batina, J. T., and Yang, H. T. Y., "Aeroelastic Analysis of Wings Using the Euler Equations with a Deforming Mesh," *Journal of Aircraft*, Vol. 28, No. 11, 1991, pp. 781–788.

[17]Lamb, H., *Hydrodynamics*, 6th ed., Dover, New York, 1932, Chap. IX, pp. 363–475.